Journal of Materials Science: Materials in Electronics (2020) 31:8174–8182
https://doi.org/10.1007/s10854-020-03314-w

Effects of electrolyte on micro-structure and properties of $Ba_xSr_{(1-x)}TiO_3$ films prepared by micro-arc oxidation

Min Wang[1,2] · Xi Zuo[1] · Kang Li[2] · Kang Wang[3]

Received: 12 February 2020 / Accepted: 24 March 2020 / Published online: 2 May 2020

Abstract
$Ba_xSr_{(1-x)}TiO_3$(BST) films are deposited on titanium substrate by micro-arc oxidation (MAO) technique under three electrolytes. The micro-structure and electrical properties of the BST thin films are analyzed and compared. The results show that the BST films obtained with these three electrolytes are all mainly composed of tetragonal $Ba_xSr_{(1-x)}TiO_3$. Compared with electrolyte without additive, both PVP30 and EDTA, as additive, significantly inhibit the growth of BST films, and the BST films become flat and dense. Moreover, the dielectric and ferroelectric properties of BST thin films are positively correlated with their micro-structure, and flat and dense BST film possesses good dielectric and ferroelectric properties. The residual polarization intensity of BST film prepared with the electrolyte involving PVP30 or EDTA is about 18 and 13 times of that of BST film prepared without additive, respectively.

1 Introduction

$Ba_xSr_{(1-x)}TiO_3$ (BST) is one of the new functional materials intensively attended due to its high dielectric constant, low dielectric loss, adjustable Curie temperature, and stable structure [1, 2]. Up to now, four common pathways, including magnetron sputtering [3, 4], sol–gel [5, 6], pulse laser deposition [7, 8], and metal organic chemical vapor deposition [9, 10], are disclosed to prepare BST films. Although these methods have their own advantages and characteristics, they suffer from different drawbacks that hamper the large-scale commercial applications of BST films [11–13]. Therefore, development of new approaches to fabricate BST films with controllable chemical composition and good uniformity is a huge challenge. Moreover, preparation of BST films under post-heat treatment-free conditions with fast deposition at a low processing temperature over large areas is demanded.

Micro-arc oxidation (MAO) is a kind of surface modification technique, which can in situ form ceramic coatings on the surface of some nonferrous metals. With the advantages of fast film deposition, simple operation, adjustable film composition, metallurgical bonding between the thin film and substrate, no pollution, and no need to post-heat treatment, MAO is expected as a new low-cost technology to prepare BST ferroelectric thin films over a large scale [14–16]. The previous research revealed that BST films deposited in situ on a Ti substrate by MAO in a solution of $Ba(OH)_2$ and $Sr(OH)_2$ bring about a big surface roughness due to the existence of defects, such as particles and cracks, which seriously affect the smoothness and compactness of films. As a result, a small dielectric constant and a large dielectric loss value would be achieved for the obtained BST film. It is generally believed that the dielectric properties of the film depend on the micro-structure and interface between thin film and electrode. A dense and crack-free film bears a uniform grain size with a small film roughness and is prone to gain improved dielectric properties [7, 17–19]. However, up to now, most of the researches on the MAO preparation of BST thin films are focused on the influence of micro-arc oxidation process parameters on the micro-structure, surface morphology, and dielectric properties of films. Optimization of the preparation process of BST thin films by MAO, especially optimization of the micro-arc oxidation electrolyte, needs further investigation in depth. In this paper, the MAO electrolyte is optimized by adding some additives and the

✉ Min Wang
wangmin@gpnu.edu.cn

[1] College of Mechanical Engineering, Guangdong Polytechnic Normal University, Guangzhou 510635, China

[2] School of Materials Science and Engineering, South China University of Technology, Guangzhou 510641, China

[3] School of Materials Science and Engineering, DongGuan University of Technology, Dongguan 523808, China

effects of PVP30 and EDTA, as additives, are detected on the micro-structure, morphology, and dielectric properties of the BST films. It is hoped to achieve high performance by optimizing the micro-structure at special electrolyte. More importantly, the authors demonstrated an efficient and low-cost MAO deposition method for obtaining the BST thin films with excellent ferroelectric property.

2 Experimental

2.1 BST samples preparation

The Ti plate (99.6%) was cut into small pieces with a dimension of 40 mm × 20 mm × 2 mm and, then, mechanically abraded using emery paper up to 1000 grits. Subsequently, the samples were degreased with an acidic mixture of HF-HNO_3 (1:3 vol.%). The degreased substrates were sequentially washed with acetone and distilled water and, then, dried in an oven. The JYW-50 micro-arc oxidation power was used in these experiments. The Ti substrate was served as the anode and a stainless steel plate selected as cathode. The electrolytic solutions were prepared as $Ba(OH)_2{\cdot}8H_2O$ (0.6 M) + $Sr(OH)_2{\cdot}8H_2O$ (0.4 M), $Ba(OH)_2{\cdot}8H_2O$ (0.6 M) + $Sr(OH)_2{\cdot}8H_2O$ (0.4 M) + PVP30 (0.02 M), and $Ba(OH)_2{\cdot}8H_2O$ (0.6 M) + $Sr(OH)_2{\cdot}8H_2O$ (0.4 M) + EDTA (0.06 M). BST thin films constructed under these three electrolyte solutions were defined as BST-NO, BST-PVP30, and BST-EDTA, respectively. The current density of micro-arc oxidation was set as 0.5 A/cm^2, current frequency of 150 Hz, the reaction time of 15 min, and the duty ratio of 85%. The electrolyte temperature was controlled by a circulating water at 50 − 60 °C during the process.

2.2 Micro-structure and performance characterization

The micro-structure of BST films was examined using a high-resolution field emission scanning electron microscope (SEM, Nova Nano430).The surface roughness of thin films was measured by a German BMT Exert 3D tomography. Each sample was measured horizontally and vertically at three different positions with a scan length of 10 mm, respectively, and the surface roughness value was attained as the average value of six tests. The thickness of the membrane was determined by the vortex thickness measuring instrument (SurfixF, PHYNIX). The crystal structure and phase composition of BST films were analyzed by an X-ray diffractometer (philips X'pert MPD Pro) with a Cu-Kα target material. The wavelength (λ) was set as 1.54056 Å and scanning angle was arranged at 20 − 90° with a step speed of 0.0214°/ms. X-Ray photoelectrons spectroscopy (XPS) incorporating a Kratos Ultra Axis spectrometer equipped with a mono-chromatized Al-Kα X-ray source (1486.6 eV) was used to analyze the chemical composition of the BST membrane and the binding states. The electron analyzer was utilized in a constant analyzer energy mode using a full and a narrow spectral pass energy of 160 and 40 eV, respectively. Peak analyses were performed using the XPS Peak 41 Software. The energy scale was calibrated by assigning the energy of 284.6 eV to the C 1s peak, corresponding to the adventitious carbon. Agilent HP4284 high-precision impedance analyzer equipped with a fast 16334A test fixture was used to measure the capacitance and dielectric loss of the films at the test voltage of 1.0 V and test frequency of 20 to 1×10^6 Hz. The polarization *vs.* electric field (*P–E*) hysteresis characteristics were obtained using a Radiant Precision LC material analyzer. Before measurement, a Pt electrode with a diameter of 10 mm was sputtered on the surface of BST film by a high-vacuum plating apparatus (Leica EM SCD500).

3 Results and discussion

3.1 Structural analysis

The SEM results of BST films derived from different electrolytic liquid systems are presented in Fig. 1. As can be seen, the smoothness and compactness of the films are effectively improved by the electrolyte involving PVP30 or EDTA. The BST-NO film shows a large number of volcanic pores and particles on the surface. The diameter of micro-arc oxidation hole is large, about 4–10 μm. There are also cracks on the surface of film, which leads to a poor smoothness and compactness of the film. The surface roughness is large, about 4.00 μm, as displayed in Fig. 1a. The SEM surface morphology of the BST-PVP30 film is depicted in Fig. 1b. The micro-arc oxidation hole with a diameter of about 200–700 nm is distributed on the film surface, and the surface roughness value is reduced to about 0.43 μm. Cracks and coagulated mass are still widely distributed on the surface. The surface appearance of BST-EDTA thin film is shown in Fig. 1c. Micro-arc oxidation pores with the size of about 500–1500 nm are evenly distributed on the surface of film, and many pod-like particles can be observed. The surface roughness is further reduced to about 0.38 μm. Therefore, it can be envisaged that both PVP30 and EDTA can improve the quality of the films.

According to the literatures [20–23], the reasons why the addition of PVP30 can make the film smooth and dense is as follows: on the one hand, lactam in PVP molecules is a strong polar group, with hydrophilic ability, can absorb a large number of water molecules, and has a good water retention ability, thus increasing the elasticity of the film; on the other hand, nitrogen-containing heterocyclic rings in PVP molecules can form complexes with Ba^{2+} and Sr^{2+} ions in

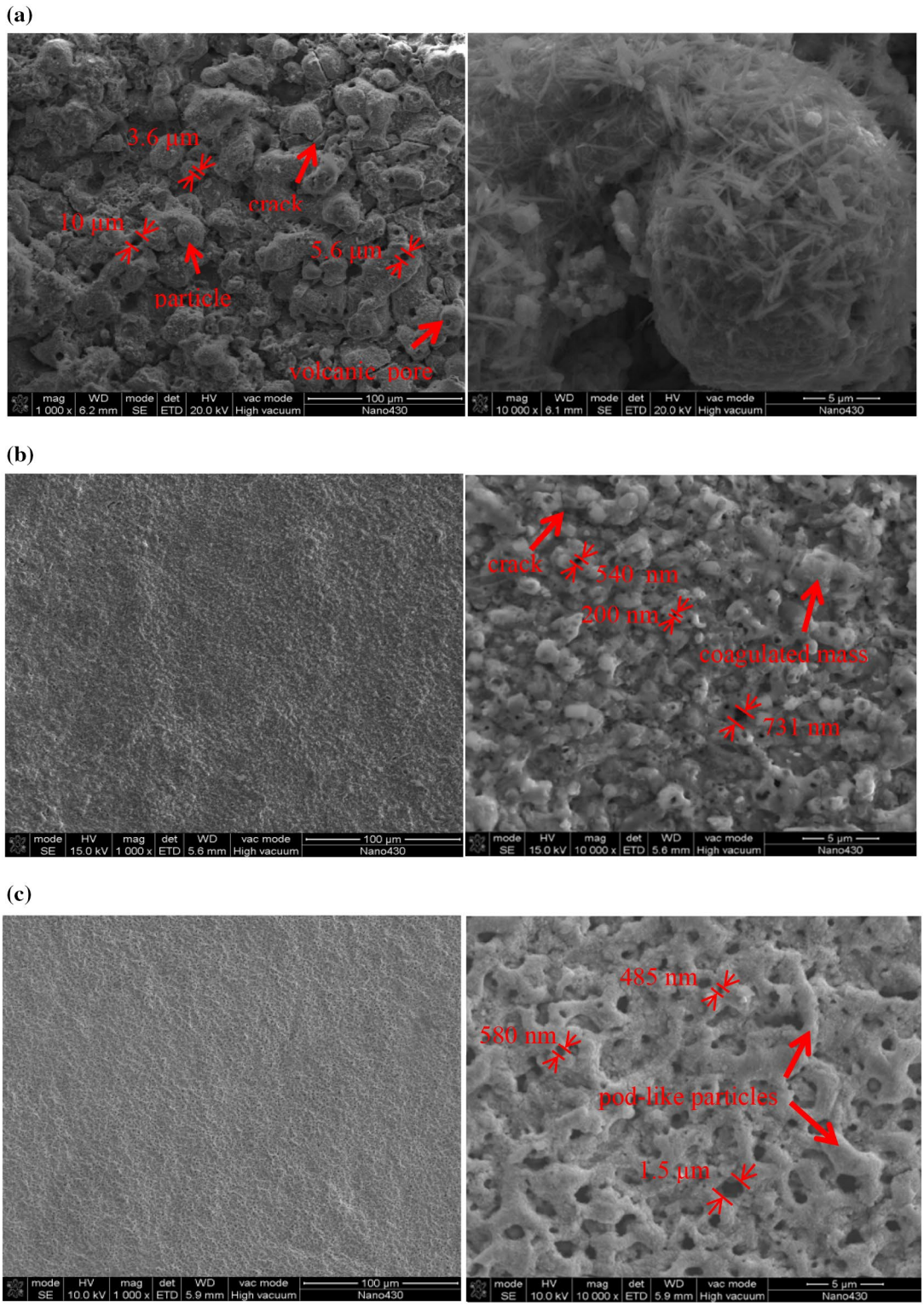

Fig. 1 SEM figures of the BST-NO (**a**), BST-PVP30 (**b**) and BST-EDTA (**c**) thin films

the electrolyte and adsorb on the surface of Ti matrix, thus slowing down the micro-arc oxidation reaction, reducing the stress in the film and inhibiting the generation of cracks. In strong alkaline solutions, EDTA mainly exists in the form of Y^{4-} [24], which can react with Ba^{2+} and Sr^{2+} to form the corresponding complexes of EDTA [25, 26]. This chelate ligand has a large steric hindrance, which retards the oxidation of Ti substrate and slows down the MAO reactions [27–29], thus inhibiting the growth of the film, resulting in obtaining the flat and dense films. The thicknesses of the BST-NO, BST-PVP30, and BST-EDTA thin films are shown in Fig. 2. It can be seen that the thickness of BST-PVP30 or BST-EDTA thin film is about one-fifth of that of the BST-NO.

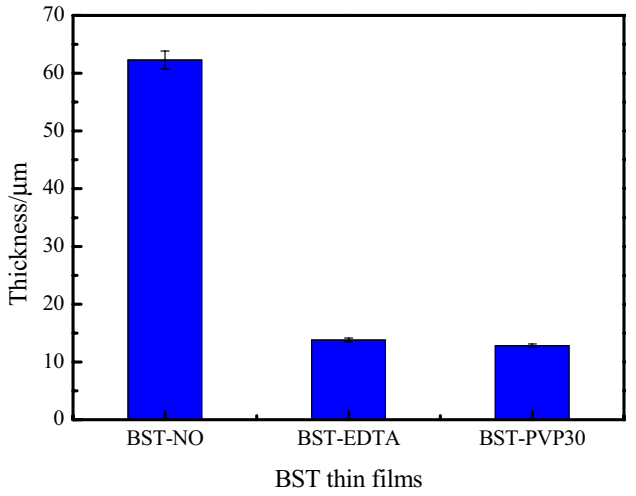

Fig. 2 The thicknesses of the BST-NO, BST-PVP30 and BST-EDTA thin films

3.2 XRD analysis

The XRD patterns of BST thin films are shown in Fig. 3. Findings reveal that the obtained BST films are mainly composed of perovskite $Ba_xSr_{(1-x)}TiO_3$, minimal (Ba, Sr)CO_3, and TiO_2 phases. This observation indicates that addition of PVP30 or EDTA in the electrolyte solution does not affect the phase composition of BST films. The (Ba, Sr)CO_3 phase is thought to be produced by the reaction of $Ba(OH)_2$ and $Sr(OH)_2$ with CO_2 in the air during micro-arc oxidation and enters into the membrane layer through the discharge channel [30]. TiO_2 is indicated as an intermediate phase in the micro-arc oxidation reaction. At the beginning of micro-arc oxidation reaction, titanium was dissolved and oxygen evolved at the anode. Some of the produced oxygen was released as O_2 gas, while the remaining dissolved in the electrolyte and produced O^{2-} [27–29]. Then, the generated oxide ion reacted with Ti^{4+} to form titanium dioxide. When PVP30 or EDTA is added into the electrolyte, diffraction peaks due

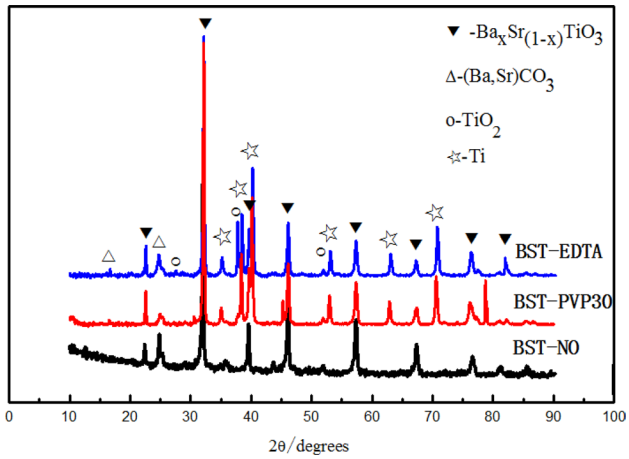

Fig. 3 XRD patterns of the BST films

to the metallic Ti substrate are appeared in the XRD pattern of film. Therefore, it can be declared that both PVP30 and EDTA have an inhibitory effect on the growth of film such that thickness of the film is significantly reduced and the X-ray is penetrated into the film layer [15, 20–23], which is consist with that shown in Fig. 2.

As shown in Figs. 4 and 5, variations in element information on the BST-PVP30 and BST-EDTA thin films are analyzed by XPS. XPS spectra of the BST films record C to be present in the films, as well as Ba, Sr, Ti, and O (Figs. 4a and 5a). The high-resolution XPS spectra of C 1s, Ba 3d, Sr 3d, Ti 2p, and O 1s peaks in BST-PVP30 thin film are shown in Fig. 4b–f, respectively. The spectra of C 1s (Fig. 4b) reveals two peaks with binding energies of 284.6 and 288.3 eV, respectively. The peak at 284.6 eV is assigned to the adsorbed C from the atmosphere. The peak at 288.3 eV is attributed to the C–O bonds of $SrCO_3$ and $BaCO_3$ [31, 32]. Figure 4c shows the spectrum of Ba 3d. Each of the Ba $3d_{3/2}$ and Ba $3d_{5/2}$ peaks can be fitted by two peaks separated by around 1.5 ± 0.1 eV. The lower binding energy peaks, i.e., 794.6 and 779.4 eV, are assigned to Ba atoms in the BST perovskite phase. The peaks at 796.0 and 780.8 eV are thought to be caused by Ba atoms in a decomposed carbonate. The spectrum of Sr 3d (Fig. 4d) also can be fitted into four peaks with the binding energies of 133.1, 134.0, 134.9, and 135.8 eV, respectively. The lower binding energy pair (133.1 and 134.9 eV) is assigned to Sr atoms in the perovskite phase. The higher binding energy pair (134.0 and 135.8 eV) is attributed to Sr atoms of carbonate. Figure 4e depicts the XPS spectrum of Ti 2p, which can be deconvoluted into two peaks at a combined energy of 463.5 and 458.2 eV, respectively, which are corresponded to Ti $2p_{1/2}$ and Ti $2p_{3/2}$ peaks. The binding energy of O 1s (Fig. 4f) is 532.0 eV which is consistent with the O 1s in $SrCO_3$ (532.2 eV) and $BaCO_3$ (532.2 eV). The 531.4 eV peak

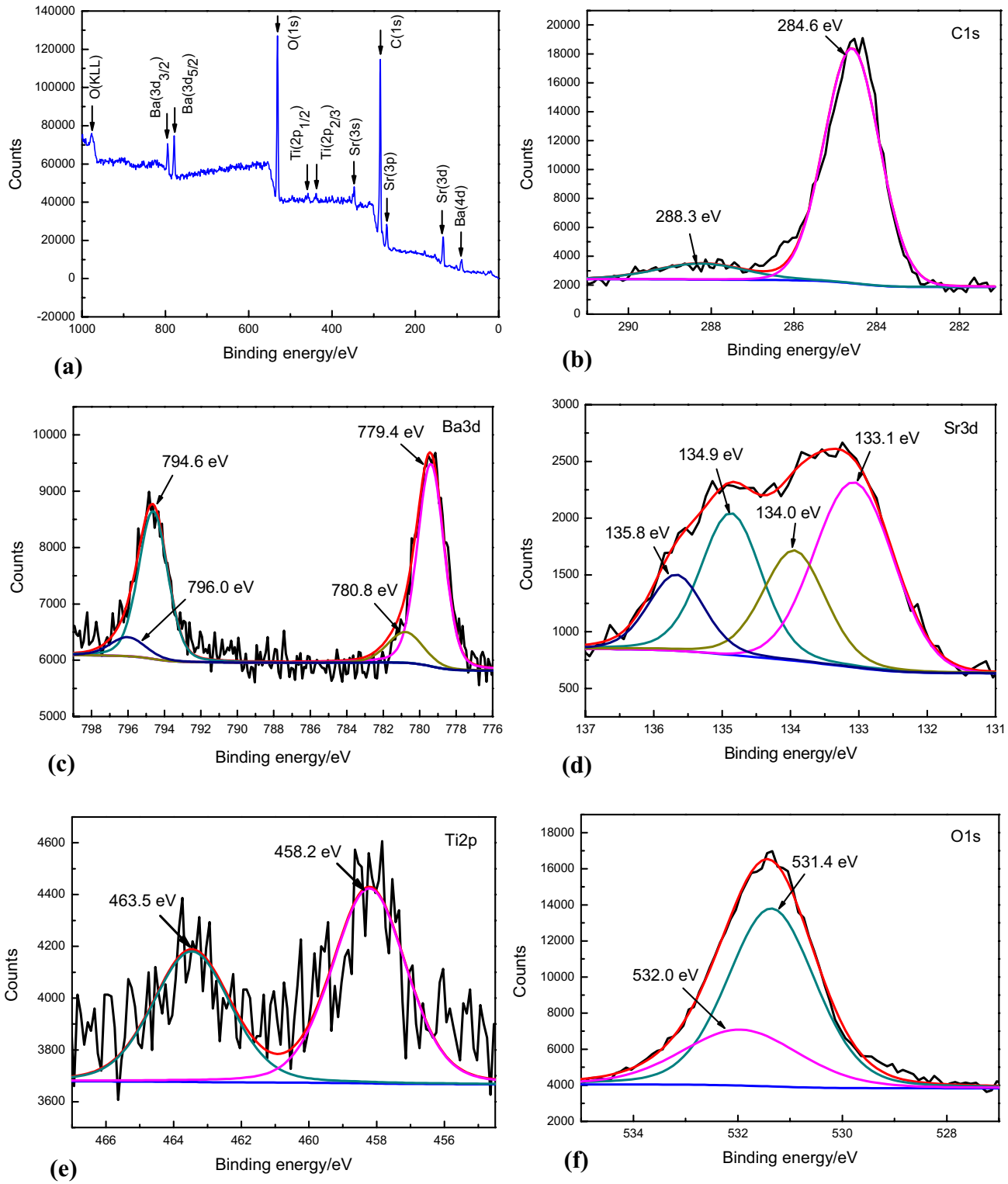

Fig. 4 XPS spectrum of the BST-PVP30 film (**a**), the XPS chemical states of C 1s (**b**), Ba 3d (**c**), Sr 3d (**d**), Ti 2p (**e**), and O 1s (**f**)

is consistent with the binding energy of O atoms in the perovskite phase. The high-resolution XPS spectra of C 1s, Ba 3d, Sr 3d, Ti 2p, and O 1s peaks in BST-EDTA thin film are shown in Fig. 5b–f respectively, which are similar to the spectra in BST-PVP30 thin film. In summary, the valence states of Ba, Sr, Ti, and O elements

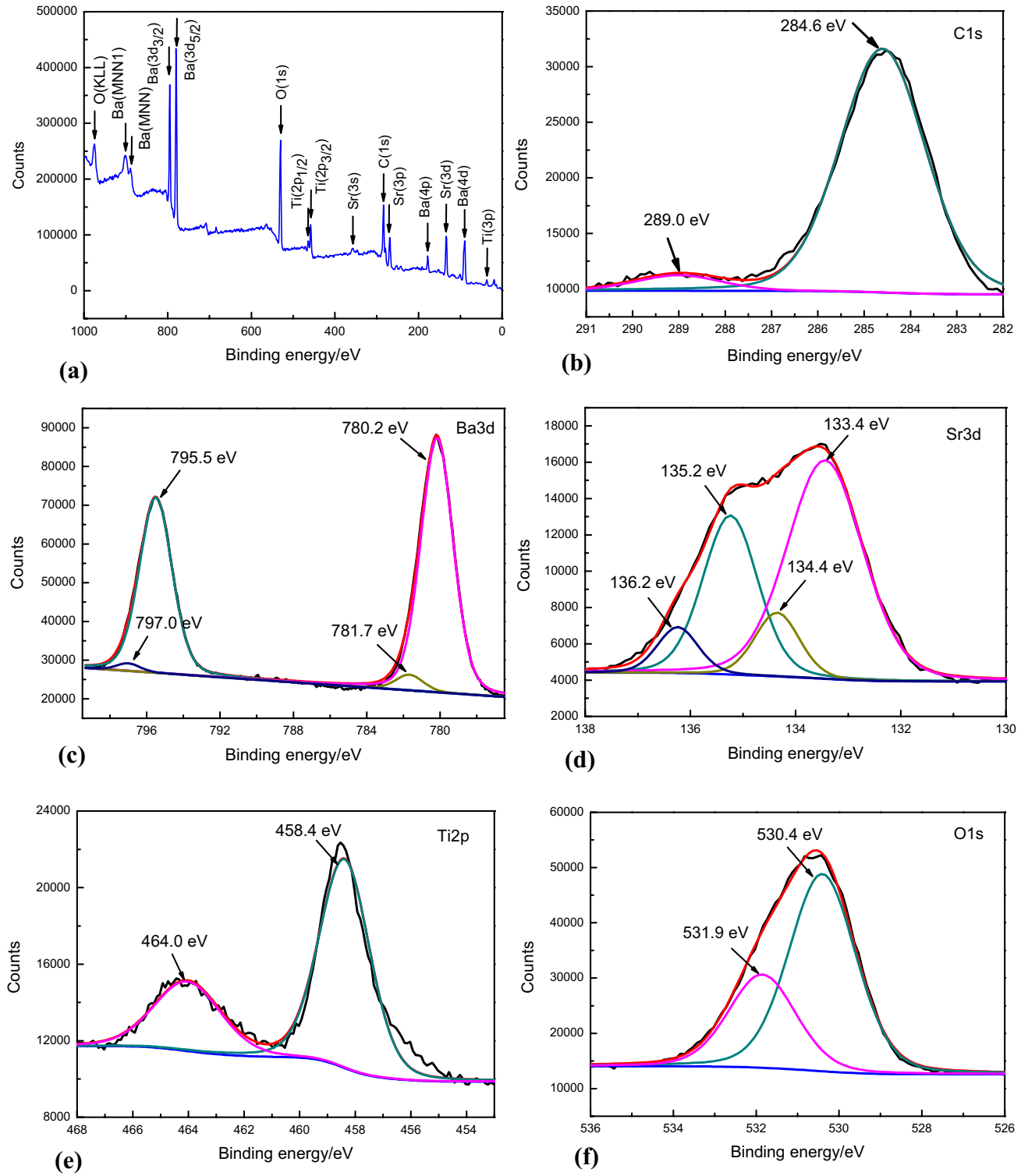

Fig. 5 XPS spectrum of the BST-EDTA film (**a**), the XPS chemical states of C 1s (**b**), Ba 3d (**c**), Sr 3d (**d**), Ti 2p (**e**), and O 1s (**f**)

in BST-PVP30 and BST-EDTA films are Ba^{2+}, Sr^{2+}, Ti^{4+} , and O^{2-}, respectively. Both BST-PVP30 and BST-EDTA membranes are mainly composed of the tetragonal $Ba_xSr_{(1-x)}TiO_3$ and carbonate, which is consistent with the results of XRD.

3.3 Dielectric properties analysis

The dielectric constants of BST films are shown in Fig. 6a. The results reveal that dielectric constant is drastically changed with frequency in the case of BST-NO film, while the mentioned changes are smooth for the BST films prepared in the presence of PVP30 and EDTA. According to the literatures [33, 34], the sharp decrease in the dielectric constant at low frequencies could be attributed to the DC conductivity and space charge polarization, which have significant contributions at low-frequency dielectric response in the films. As the frequency increases, these dipoles due to space charges do not respond, resulting in decrease in the dielectric constant. Moreover, the space charge polarization is inherently related to nonuniform charge accumulation at the grain boundaries and the film/electrode interface.

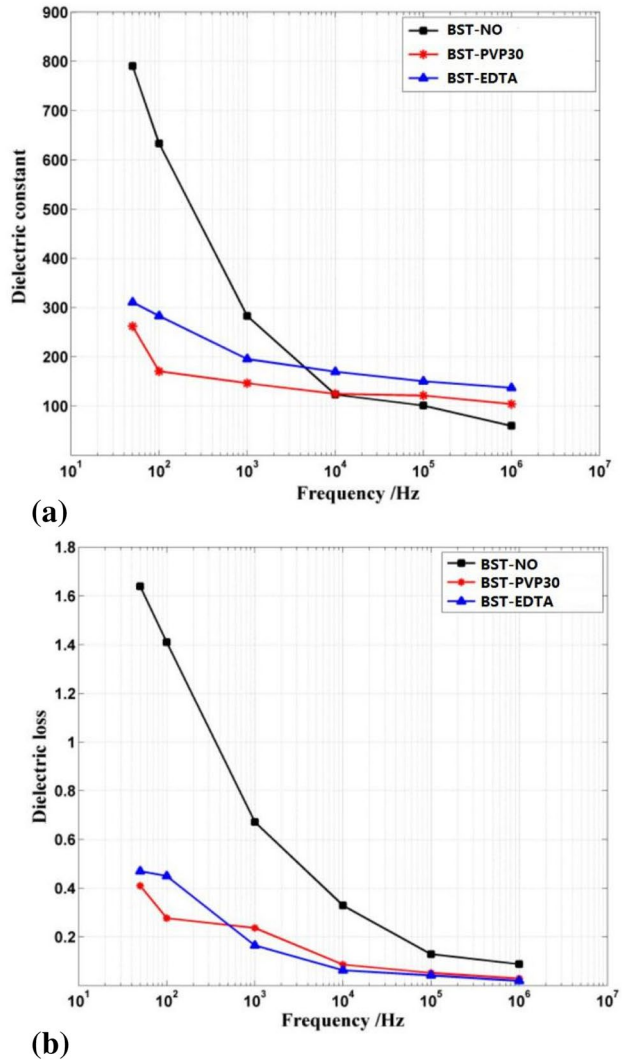

Fig. 6 Dielectric properties of the BST films: dielectric constants (**a**) and dielectric loss (**b**)

Figure 1 shows that the BST-NO film has the most defects and the largest surface roughness among three kinds of BST films. Therefore, at low frequencies, the frequency dependence of its dielectric constant is stronger than the other two films. The high dielectric loss at low frequency in this film confirms the presence of space charges at the film/electrode interface. The dielectric loss analysis of the three BST films is shown in Fig. 6b. The results confirm that the dielectric loss of all films are decreased with enhancing frequency within the range of $50 - 1 \times 10^6$ Hz, and the dielectric losses of BST-PVP30 and BST-EDTA films are significantly lower than that of BST-NO film. Moreover, the dielectric loss of BST-EDTA film is lower than that of BST-PVP30 film when a higher frequency greater than 500 Hz was used. For example, under the condition of 1 kHz, the dielectric losses of BST-PVP30 and BST-EDTA films are 0.237 and 0.165, respectively, confirming about 30% decrease after addition of EDTA. According to Eq. (1), the dielectric constant of a film is directly proportional to the measured capacitance and film thickness under the same electrode area. The thickness of BST-NO film is about five times greater than those of BST-PVP30 and BST-EDTA films, while the differences in dielectric constants are less than three times for these films, even at the maximum value. This finding proves that capacitance of the thin films prepared in the presence of PVP30 and EDTA is significantly increased. In addition, as shown in Fig. 1, the sample derived from an electrolyte involving EDTA or PVP30 exhibits the low roughness and improved compactness, in agreement with the large dielectric constant and small dielectric loss value. This observation demonstrates that the dielectric properties of BST thin films are positively correlated with their micro-structure.

$$\varepsilon' = \frac{C \times d}{\varepsilon_0 \times S}, \tag{1}$$

where C is the electrical capacity (F) of sample, S is the electrode area (7.854×10^{-5} m^2), d is the thickness of (m), and ε_0 is the vacuum dielectric constant (8.85×10^{-12} F/m).

3.4 Ferroelectric performance analysis

The hysteresis loops of BST thin films are measured under the voltage of 700 V and frequency of 20 Hz, as shown in Fig. 7. The hysteresis loops of all three BST films present ferroelectric features, but none is closed, which may be caused by the residual stress and depolarization field in the film [35]. In addition, it can be seen that the residual polarization intensity decreases significantly as the voltage increases as shown in Fig. 7a, which is mainly related to the oxygen vacancy in the membrane [36–38]. According to the literatures [39, 40], in the ABO_3-type oxides, oxygen atoms

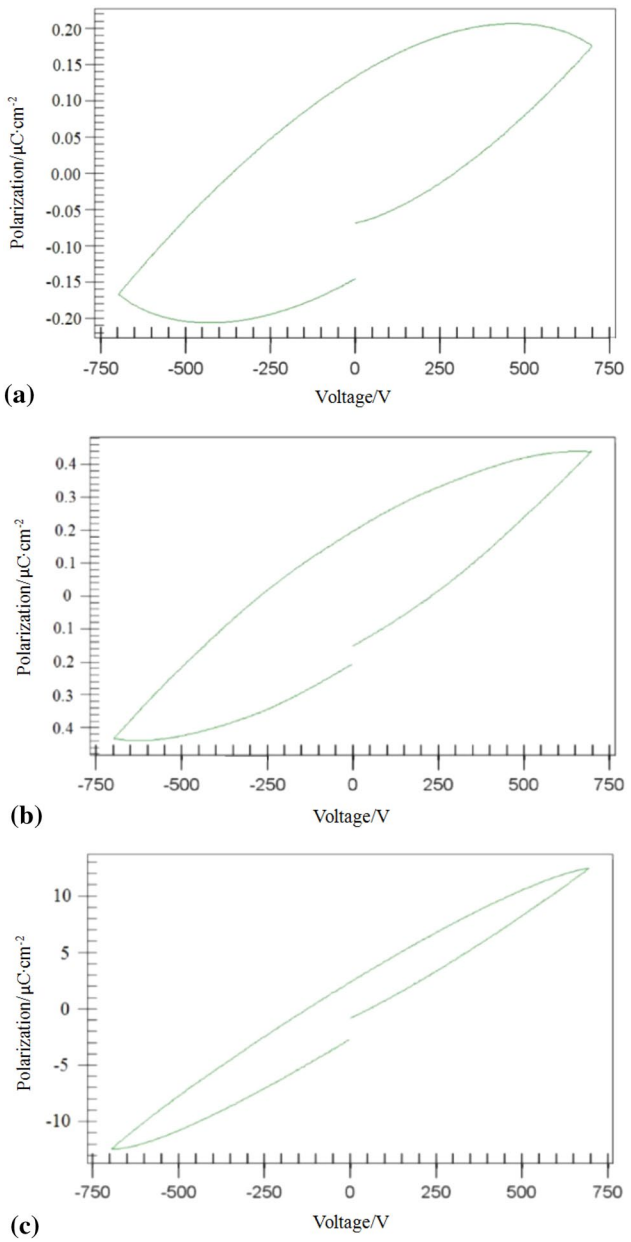

Fig. 7 Electric hysteresis loops of the BST-NO (**a**), BST-PVP30 (**b**), and BST-EDTA (**c**) thin films

escaped from the lattice structure to form oxygen vacancies, which pinned the inversion of the ferroelectric domains. With the increase of voltage, oxygen vacancies increased and the pinning effect on ferroelectric domains was strengthened, so the ferroelectric domains could not be reversed in time, and the residual polarization strength of films decreased. The ferroelectric properties of these three BST films are shown in Table 1. Obviously, the residual polarization intensities of BST-EDTA film and BST-PVP30 film is about 18 and 13 times of that of BST-NO film, respectively. Combined with Fig. 1, it can be concluded that the ferroelectric property of the film is also closely related to the micro-structure, such that a flat and compact film can provide an improved ferroelectric property. This is in agreement with the results reported in the literatures [7, 19].

Table 1 The residual polarization and coercive field strengths of the BST thin films

BST films	Residual polarization/ $\mu C \cdot cm^{-2}$		Coercive field strength/ $kV \cdot cm^{-1}$	
	P_r	$-P_r$	E_c	$-E_c$
BST-NO	0.14	−0.14	46.7	−58.5
BST-PVP30	0.2	−0.2	181.7	−220.4
BST-EDTA	2.5	−2.5	40.0	−92.4

4 Conclusions

This study shows that the micro-structure and dielectric properties of a BST film prepared by micro-arc oxidation can be improved by adding additives into the electrolyte. Both PVP30 and EDTA have inhibitory effect on the growth of the BST film, so that the thickness of the BST thin film is significantly reduced. Compared with the BST-NO thin film, the micro-arc oxidation pores of the BST-PVP30 and BST-EDTA films are evenly distributed, the surface roughness is reduced to about 0.4 μm, and the film becomes more flat and dense. The addition of EDTA or PVP30 improves the micro-structure of BST film and increases the capacitance value of BST film, thus offsetting the negative influence of the film thickness reduction on the dielectric constant of the film and reducing the dielectric loss. It also contributes to the improvement of ferroelectric property of BST thin film. These findings may provide valuable insights on the preparation of low-cost BST films with large area and high quality.

Acknowledgements This study was supported by the Science and Technology Planning Project of Guangdong Province (No.2016A010103040), the Educational Commission of Guangdong Province (No.2015KTSCX084).

References

1. Yu Yang, X. Wang, Xi Yao, Dielectric properties of $Ba_{1-x}Sr_xTiO_3$ ceramics prepared by microwave sintering. Ceram. Int. **39**, S335–S339 (2013)
2. C. Liu, P. Liu, Microstructure and dielectric properties of BST ceramics derived from high-energy ball-milling. J. Alloy. Compd. **584**, 114–118 (2014)
3. A.V. Tumarkin, S.V. Razumov, A.G. Gagarin, A.A. Odinets, A.K. Mikhailov, I.P. Pronin, V.M. Stozharov, S.V. Senkevich, N.K. Travin, Ferroelectric films of barium strontium titanate on

semi-insulating silicon carbide substrates. Tech. Phys. Lett. **42**, 423–426 (2016)
4. C.-H. Lee, Oh Young-Jei, Deuk Yong Lee, Doo-Jin Choi, Influence of annealing temperature on the dielectric properties of $BaSrTiO_3$ thin films deposited on various substrates. J. Korean Phys. Soc. **69**, 1571–1574 (2016)
5. P. Ge, X. Tang, Q. Liu, Y. Jiang, W. Li, J. Luo, Energy storage properties and electrocaloric effect of $Ba_{0.65}Sr_{0.35}TiO_3$ ceramics near room temperature. J. Mater. Sci. **29**, 1075–1081 (2018)
6. A. Elbasset, S. Sayouri, F. Abdi, T. Lamcharfi, L. Mrharrab, Effect of Sr addition on piezoelectric properties and the transition temperature of $BaTiO_3$. Glass Phys. Chem. **43**, 91–97 (2017)
7. Z. Saroukhani, N. Tahmasebi, Seyed Mohammad Mahdavi, Ali NEMATI, Effect of working pressure and annealing temperature on microstructure and surface chemical composition of barium strontium titanate films grown by pulsed laser deposition. Bull. Mater. Sci. **38**, 1645–1650 (2015)
8. J.P.B. Silva, A. Khodorov, A. Almeida, J.A. Moreira, M. Pereira, M.J.M. Gomes, $Ba_{0.8}Sr_{0.2}TiO_3$ films crystallized on glass and platinized substrates by laser-assisted annealing at room temperature. Appl. Phys. A. **116**, 1271–1280 (2014)
9. N.M. Sbrockey, M.W. Cole, T.S. Kalkur, M. Luong, J.E. Spanier, G.S. Tompa, MOVCD growth of compositionally graded $Ba_xSr_{1-x}TiO_3$ thin films. Integr. Ferroelectr. **126**, 21–27 (2011)
10. Y. Sakabe, Y. Takeshima, K. Tanaka, Multilayer ceramic capacitors with thin (Ba, Sr)TiO_3 layers by MOCVD. J. Electroceram. **3**, 115–121 (1999)
11. D. Yan, L. Luo, Y. Zhang, Z. Peng, H. Liu, D. Xiao, T. Liu, X. Lai, J. Zhu, Influence of deposition temperature on microstructure and electrical properties of modified (Ba,Sr)TiO_3 ferroelectric thin films. Ceram. Int. **41**, S520–S525 (2015)
12. G. Shuster, O. Kreinin, E. Lakin, N.P. Kuzmina, E. Zolotoyabko, MOCVD growth of barium-strontium titanate films using newly developed barium and strontium precursors. Thin Solid Films **518**, 4658–4661 (2010)
13. S. Xiao, W. Jiang, K. Luo, J. Xia, L. Zhang, Structure and ferroelectric properties of barium titanate films synthesized by sol–gel method. Mater. Chem. Phys. **127**, 420–425 (2011)
14. M. Tezua, M. Iwasaki, Plasma-induced degradation of aniline in aqueous solution. Thin Solid Films **386**, 204–207 (2001)
15. Y.-K. Shin, W.-S. Chae, Y.-W. Song, Y.-M. Sung, Formation of titania photocatalyst films by microarc oxidation of Ti and Ti6Al4V alloys. Electrochem. Commun. **8**, 465–470 (2006)
16. M.-H. Hong, D.-H. Lee, K.-M. Kim, Y.-K. Lee, Study on bioactivity and bonding strength between Ti alloy substrate and TiO_2 film by micro-arc oxidation. Thin Solid Films **519**, 7065–7070 (2011)
17. M. Shahbazi, A. Bahari, S. Ghasemi, Structural and frequency-dependent dielectric properties of PVP-SiO_2-TMSPM hybrid thin films. Org. Electron. **32**, 100–108 (2016)
18. A. Bahari, M. Shahbazi, Electrical properties of PVP-SiO_2-TMSPM hybrid thin films as OFET gate dielectric. J. Electron. Mater. **45**, 1201–1209 (2016)
19. J.X. Liao, C.R. Yang, Z. Tian, H.G. Yang, L. Jin, The influence of post-annealing on the chemical structures and dielectric properties of the surface layer of $Ba_{0.6}Sr_{0.4}TiO_3$ films. J. Phys. D **39**, 2473 (2006)
20. Z. Wang, J. Liu, T. Ren, L. Liu, Fabrication of organic PVP doping-based $Ba_{0.5}Sr_{0.5}TiO_3$ thick films on silicon substrates for MEMS applications. Sensor. Actuat. A: Phy. **117**, 293–300 (2005)
21. A. Gómez-Acosta, E.J. Manzano-Ramírez, L.M. López-Naranjo, R. Apatiga, E.M. Herrera-Basurto, Rivera-Muñoz, silver nanostructure dependence on the stirring-time in a high-yield polyol synthesis using a short-chain PVP. Mater. Lett. **138**, 167–170 (2015)
22. Yu Lei, W.-L. Liu, Z.-F. Zhang, Z.-T. Song, Synthesis of colloid silica coated with ceria nano-particles with the assistance of PVP. Chinese Chem. Lett. **26**, 700–704 (2015)
23. J.D. Corbett, S. von Winbush, F.C. Albers, The solubility of the post-transition metals in their molten halides. J. Am. Chem. Soc. **79**, 3020–3024 (1957)
24. R. Pribil, *Analytical applications of EDTA and related compounds: international series of monographs in analytical chemistry* (Pergamon Press, Oxford, 1972)
25. M.A. Earl, *Critical stability constants* (Plenum Press, New York, 1974)
26. S. Chen, S. Hoffmann, Y. Prots, J.-T. Zhao, R. Kniep, Preparation, crystal structures and thermal decomposition of Ba_2(EDTA) and Ba_2(EDTA)·2.5H_2O. Z. Anorg. Allg. Chem. **636**, 1710–1715 (2010)
27. M. Shokouhfar, C. Dehghanian, M. Montazeri, A. Baradaran, Preparation of ceramic coating on Ti substrate by plasma electrolytic oxidation in different electrolytes and evaluation of its corrosion resistance: part II. Appl. Surf. Sci. **258**, 2416–2423 (2012)
28. J. Schreckenbach, F. Schlottig, G. Marx, W.M. Kriven, O.O. Popoola, M.H. Jilavi, S.D. Brown, Preparation and microstructure characterization of anodic spark deposited barium titanate conversion layers. J. Mater. Res. **14**, 1437–1443 (1999)
29. A.L. Yerokhin, X. Nie, A. Leyland, A. Matthews, S.J. Dowey, Plasma electrolysis for surface engineering. Surf. Coat. Tech. **122**, 73–93 (1999)
30. M. Wang, G. Zhang, W. Li, X. Wang, Microstructure and properties of $BaTiO_3$ ferroelectric films prepared by DC micro arc oxidation. Bull. Korean Chem. Soc. **36**, 1178–1182 (2015)
31. V. Craciun, R.K. Singh, Characteristics of the surface layer of barium strontium titanate thin films deposited by laser ablation. Appl. Phys. Lett. **76**, 1932–1934 (2000)
32. Z. Gao, Z. Jia, J. Zhang, A. Feng, Z. Huang, Wu Guanglei, Tunable microwave absorbing property of La_xFeO_3/C by introducing site cation defciency. J. Mater. Sci. Mater. Electron. **30**, 13474–13487 (2019)
33. H.B. Sharma, Structure and properties of BT and BST thin films. Ferroelectrics **453**, 113–121 (2013)
34. T. Mazon, M.A. Zaghete, J.A. Varela, E. Longo, Barium strontium titanate nanocrystalline thin films prepared by soft chemical method. J. Eur. Ceram. Soc. **27**, 3799–3802 (2007)
35. Z. Ji, Z. He, Y. Song, K. Liu, Z. Ye, Fabrication and characterization of indium-doped p-type SnO_2 thin films. J. Cryst. Growth. **259**, 282–285 (2003)
36. J.-H. Joo, J.-M. Seon, Y.-C. Jeon, Oh Ki-Young, J.-S. Roh, J.-J. Kim, Improvement of leakage currents of Pt/(Ba, Sr)TiO_3/Pt capacitors. Appl. Phys. Lett. **70**, 3053–3055 (1997)
37. M.S. Tsai, S.C. Sun, T.Y. Tseng, Effect of oxygen to argon ratio on properties of (Ba, Sr)TiO_3 thin films prepared by radio-frequency magnetron sputtering. J. Appl. Phys. **82**, 3482–3487 (1997)
38. M. Shen, Z. Dong, Z. Gan, S. Ge, W. Cao, Oxygen-related dielectric relaxation and leakage characteristics of Pt/(Ba, Sr)TiO_3/Pt thin-film capacitors. Appl. Phys. Lett. **80**, 2538–2540 (2002)
39. C.H. Park, D.J. Chadi, Microscopic study of oxygen-vacancy defects in ferroelectric perovskites. Phys. Rev. B **57**, 961–964 (1998)
40. S. Ezhilvalavan, T.-Y. Tseng, Progress in the developments of (Ba, Sr)TiO_3 (BST) thin films for Gigabit era DRAMs. Mater. Chem. Phys. **65**, 227–248 (2000)